Journal of Crystal Growth 316 (2011) 56–59

Contents lists available at ScienceDirect

Journal of Crystal Growth

journal homepage: www.elsevier.com/locate/jcrysgro

# Properties of molecular beam epitaxially grown ScAs:InGaAs and ErAs:InGaAs nanocomposites for thermoelectric applications

X. Liu [a,*], A.T. Ramu [a], J.E. Bowers [a], C.J. Palmstrøm [a], P.G. Burke [b], H. Lu [b], A.C. Gossard [b]

[a] Department of Electrical and Computer Engineering, University of California, Santa Barbara, CA 93106-9560, USA
[b] Materials Department, University of California, Santa Barbara, CA 93106-5050, USA

ARTICLE INFO

*Article history:*
Received 2 September 2010
Received in revised form
28 September 2010
Accepted 29 September 2010
Communicated by: K.H. Ploog
Available online 15 October 2010

*Keywords:*
A1. Doping
A1. Nanostructures
A1. Nucleation
A3. Molecular Beam Epitaxy
B1. Rare earth compounds
B2. Semiconducting III–V materials

ABSTRACT

We report the molecular beam epitaxy (MBE) growth and the comparative systematic study of the electrical and thermoelectric characterizations of ScAs:$In_{0.53}Ga_{0.47}As$ and ErAs:$In_{0.53}Ga_{0.47}As$ nanocomposites. The peak room-temperature power factor of ScAs:InGaAs is 38% comparing to that of ErAs:InGaAs. The carrier concentration change of the nanocomposites versus the ScAs and ErAs incorporation levels below 2.2% is explained as due to the formation of nanoparticles with different sizes and densities. The carrier concentration difference between the two types of nanocomposites at the same incorporation level of ScAs and ErAs is explained by the size difference between the ScAs and ErAs nanoparticles.



## 1. Introduction

Semiconductors embedded with semimetallic nanoparticles are promising materials for thermoelectric applications outside the optimal temperature range of $Bi_2Te_3$ [1]. The figure of merit for thermoelectric materials has the form of $ZT=S^2\sigma T/\kappa$, where $S$ is the Seebeck coefficient, $\sigma$ is the electrical conductivity, and $\kappa$ is the thermal conductivity. The embedded semimetallic nanoparticles can provide carrier doping to increase $\sigma$, electron energy filtering to increase $S$ [2], and phonon scattering to decrease $\kappa$ [3]. When these interrelated parameters are optimized through careful materials selection and growth design, the $ZT$ of the resulting nanocomposites can be enhanced with respect to the original semiconductor matrix. Recent study has been concentrated on ErAs:InGa(Al)As nanocomposites, and a thermoelectric power generator module with an output power of 6.3 W has been fabricated [4].

However, the growth and resulting property change of embedding other rare-earth pnictides into III–Vs remains largely unexplored. Among all the rare-earth elements, Sc has the smallest atomic number and Sc mono-pnictides have the smallest lattice parameters [5]. This gives the latter an important role in the engineering of thermoelectric materials, since the incorporation of Sc-containing nanoparticles may cover a unique wavelength range of phonon scattering. Specifically, ScAs is also a semimetal with a similar band structure to the widely studied ErAs [6–8]. The solubility limit of Sc in GaAs is estimated to be on the order of $10^{17}$ $cm^{-3}$ [9], which is similar to that of Er [10,11]. $Sc_{0.32}Er_{0.68}As$ films have been grown lattice matched on (0 0 1) GaAs [5]. Here, we report the molecular beam epitaxy (MBE) growth and the comparative systematic study of ScAs:$In_{0.53}Ga_{0.47}As$ and ErAs:$In_{0.53}Ga_{0.47}As$ nanocomposites in order to illustrate their electrical and thermoelectric properties.

## 2. Experimental procedure

The ScAs:InGaAs samples were grown on semi-insulating (0 0 1)Fe:InP substrates in a VG V80H MBE system. Sc was evaporated from a solid-source high-temperature effusion cell with a tungsten crucible. Before growth the substrate was heated to 530 °C under As to desorb oxide. The temperature was subsequently lowered to 460 °C to grow a 270 nm $In_{0.53}Ga_{0.47}As$ buffer layer that is lattice matched to the InP substrate. The Sc cell was then opened for the codeposition of ScAs with InGaAs. The InGaAs growth rate was 0.81 μm/h and the film thickness was 1.8 μm. The Sc cell temperatures were kept at 1010 °C, 1025 °C, 1070 °C, 1085 °C, 1130 °C, and 1160 °C, respectively, and the Sc incorporation rate was estimated from secondary ion mass spectroscopy (SIMS) measurements after growth with the Sc signal referenced to the background As signal, which is assumed to

* Corresponding author.
*E-mail address:* xliu@ece.ucsb.edu (X. Liu).

0022-0248/$ - see front matter © 2010 Elsevier B.V. All rights reserved.
doi:10.1016/j.jcrysgro.2010.09.078

correspond to an atomic concentration of $1.0\times10^{19}\,cm^{-3}$ in the film as determined from SIMS measurements on Sc implanted GaAs samples [12]. Streaky $2\times4$ reconstruction patterns were observed by *in situ* reflection high-energy electron diffraction (RHEED) on the oxide-desorbed InP substrate, the InGaAs buffer, and the ScAs:InGaAs nanocomposites with a ScAs concentration of less than 3%. The $2\times4$ pattern on ScAs:InGaAs changed to $4\times3$ after growth when the temperature was reduced below 440 °C. The ErAs:InGaAs samples were grown in a Varian Gen II MBE system on semi-insulating (0 0 1)Fe:InP with a 100 nm $In_{0.52}Al_{0.48}As$ buffer layer. The InP oxide desorption process and the growth temperature were similar to that of ScAs:InGaAs. The InGaAs growth rate was 2 μm/h and the thickness was 2 μm. The Er cell temperatures were varied between 865 °C and 1035 °C, and the Er incorporation rate was determined from growth rate measurements. The room-temperature electrical conductivity and electron mobility were measured by the van der Pauw method using In dots as ohmic contacts. The room-temperature Seebeck coefficient was measured on a 2 mm × 10 mm sample bar along the [$\bar{1}$ 1 0] direction.

## 3. Results and discussion

Fig. 1 plots the (a) Seebeck coefficient ($S$), (b) power factor ($S^2\sigma$), (c) electrical conductivity ($\sigma$), (d) electron mobility ($\mu_n$), and (e) electron concentration ($n$) versus the ScAs and ErAs volume concentrations (ScAs% and ErAs%) for a series of ScAs:InGaAs and ErAs:InGaAs nanocomposites. The typical properties of unintentionally doped $In_{0.53}Ga_{0.47}As$ films grown in our V80H and Gen II systems are summarized in Table 1. Since the solubility limits of Sc and Er in GaAs are on the order of $10^{17}\,cm^{-3}$ [9–11], which corresponds to a volume concentration of only 0.0005%, we can assume that the amounts of Sc and Er been contained in the samples here are well beyond their solubility limits in InGaAs. This agrees with our cross-sectional scanning transmission electron microscopy (STEM) studies, from which the existence of nanoparticles have been observed at relatively low ScAs% and ErAs% of 0.66% and 0.2%, respectively, although the formation of nanoparticles may occur at even lower concentrations. Fig. 1(e) shows that the carrier concentrations increase as the ScAs% and ErAs% increase. The decrease of the carrier mobilities with increasing ScAs% and ErAs% in Fig. 1(d) is due to the increased amount of impurity scattering. The net effect is that the peak conductivities of similar values appear at 0.60% ScAs and 0.20% ErAs, as seen in Fig. 1(c). On the other hand, the Seebeck coefficient in Fig. 1(a) is directly related to the asymmetry of the differential conductive density of states with respect to the Fermi level [13], which decreases monotonically here as the carrier concentration increases. As a result Fig. 1(b) shows that the peak power factors appear at 0.35% ScAs and 0.05% ErAs, and the value of the former is about 38% of the latter.

Fig. 2 plots (a) $S$, (b) $S^2\sigma$, (c) $\sigma$, and (d) $\mu_n$ versus $n$ for the above nanocomposites together with the simulation results of Si doped InGaAs [14]. The power factor of ScAs:InGaAs nanocomposites is only slightly enhanced with respect to that of Si:InGaAs below the carrier concentration level of $1.6\times10^{18}\,cm^{-3}$. Here the benefit of increased Seebeck coefficient is offset by the decreased carrier mobility and conductivity. However the figure of merit of the former is expected to be larger than the latter due to the presence of nanoparticles, which reduces thermal conductivity via phonon scattering. Further studies including the high temperature and thermal conductivity characterizations and the cogrowth of ScErAs:InGaAs are currently in progress.

In a previous study on ErAs:InGaAs superlattice nanocomposites by Driscoll et al. [15], it was shown that the size and shape of ErAs

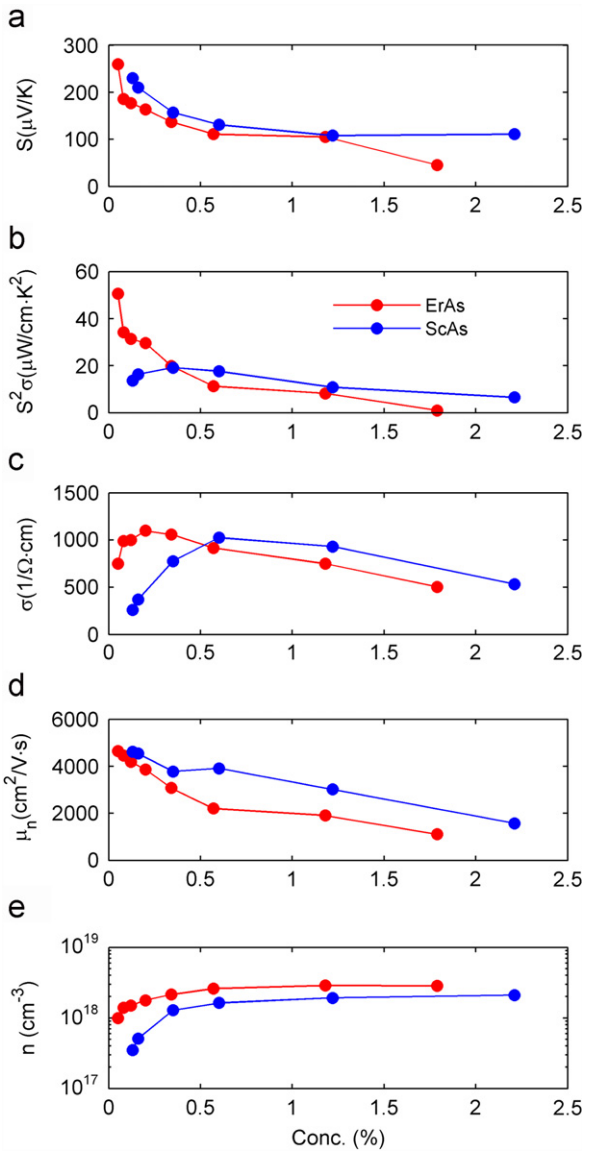


**Fig. 1.** (a) Seebeck coefficient ($S$), (b) power factor ($S^2\sigma$), (c) electrical conductivity ($\sigma$), (d) electron mobility ($\mu_n$), and (e) electron concentration ($n$) versus ScAs volume concentration (%) for ScAs:InGaAs and ErAs volume concentration (%) for ErAs:InGaAs.

nanoparticles determines the interface states and therefore affects the doping levels in the host matrix. Fig. 1(e) shows that the carrier concentrations increase more rapidly at lower incorporation levels as the ScAs% and ErAs% are increased up to about 0.35%. This indicates a critical stage of nanoparticle formation, which corresponds to the nucleation and increased spatial appearance of nanoparticles whose sizes are beyond that of the critical nucleus. Therefore the doping is enhanced and the Fermi level is lifted within the InGaAs matrix. However as the ScAs% and ErAs% are increased beyond 0.35% up to 2.2%, Fig. 1(e) shows that the carrier concentration varies slowly and gradually saturates around $2\times10^{18}\,cm^{-3}$ and $3\times10^{18}\,cm^{-3}$ for ScAs:InGaAs and ErAs:InGaAs, respectively. Accordingly, if we assume that doping is directly related to the total contact area of the nanoparticles, this suggests that the density of the nucleated nanoparticles does not increase any further, which may saturate or even decrease due to the formation of nanoparticles with larger sizes. This trend is in accord with the general theory of nucleation [16], and the coalescence of smaller ErAs nanoparticles into larger ones at

**Table 1**
Typical properties of unintentionally doped $In_{0.53}Ga_{0.47}As$ films grown in our MBE systems.

| System | $S$ ($\mu V\,K^{-1}$) | $S^2\sigma$ ($\mu W\,cm^{-1}\,K^{-1}$) | $\sigma$ ($\Omega^{-1}\,cm^{-1}$) | $\mu_n$ ($cm^2\,V^{-1}\,s^{-1}$) | $n$ ($cm^{-3}$) |
|---|---|---|---|---|---|
| V80H | 729 | 0.88 | 1.65 | 9200 | $1.1\times10^{15}$ |
| Gen II | 756 | 1.17 | 2.05 | 9100 | $1.4\times10^{15}$ |

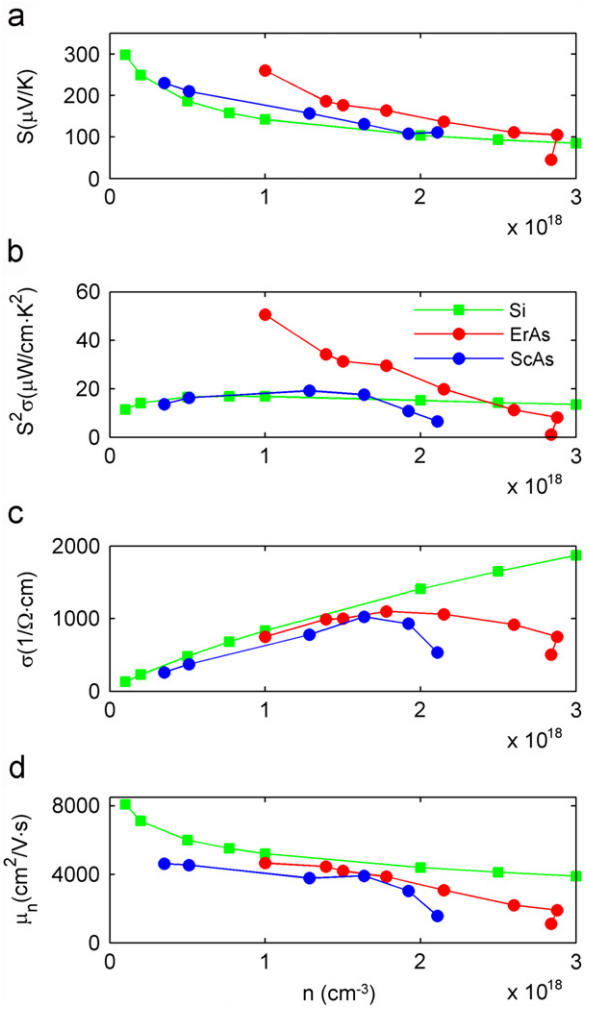


**Fig. 2.** (a) Seebeck coefficient ($S$), (b) power factor ($S^2\sigma$), (c) electrical conductivity ($\sigma$), and (d) electron mobility ($\mu_n$) versus electron concentration ($n$) for ScAs:InGaAs, ErAs:InGaAs, and Si:InGaAs.

increased ErAs incorporation levels have been observed by STEM in the case of ErAs:InGaAs [17].

Consistent with the above, we also explain the appeared relative shift of $n$ versus ScAs% and $n$ versus ErAs% in Fig. 1(e) to be due to the relatively larger size of ScAs nanoparticles than ErAs. As a result, for the same amount of volume incorporation, the total number of ScAs nanoparticles and the total contact area are less than that of ErAs. Therefore there are fewer interface states in ScAs:InGaAs, resulting lower doping levels. Meanwhile the reduction in carrier mobility is also smaller due to the reduced scattering cross-section and carrier density. Cross-sectional Transmission Electron Microscopy (TEM) has revealed that the diameter of ErAs nanoparticles in InGaAs is between 1 and 3 nm. However neither conventional TEM nor STEM is able to provide unambiguous quantitative information about the sizes of ScAs nanoparticles. In the former case the ScAs nanoparticles are not easily distinguished. In the latter case they appear as dark spots due to the smaller atomic number of Sc than In and Ga, which overlaps easily with the ion-milling lattice damages introduced during sample preparation. Other techniques such as small angle X-ray scattering (SAXS) will have to be employed. Nevertheless, *in situ* Scanning Tunneling Microscopy (STM) study of 1 monolayer deposition of ScAs and ErAs on (0 0 1)GaAs has shown that the average island diameters are 7.4 nm and 4.6 nm, respectively [18], which is larger in the former case due to the larger lattice mismatch (−3.3% for ScAs/GaAs and 1.6% for ErAs/GaAs). On the other hand, the lattice mismatches of ScAs and ErAs with respect to $In_{0.53}Ga_{0.47}As$ are −6.9% and −2.1%, respectively, and ScAs may tend to form larger nanoparticles than ErAs when embedded in InGaAs at the same incorporation levels.

## 4. Conclusions

The electrical and thermoelectric properties of the MBE grown ScAs:InGaAs and ErAs:InGaAs nanocomposites are studied systematically and comparatively. ScAs:InGaAs may be used as an alternative thermoelectric material to ErAs:InGaAs, although the peak room-temperature power factor of the former is only 38% of the latter. The carrier concentration change of the nanocomposites versus the ScAs and ErAs incorporation levels is explained as due to the formation of nanoparticles with different sizes and densities. The carrier concentration difference between the two types of nanocomposites at the same incorporation level of ScAs and ErAs is explained by the size difference between the ScAs and ErAs nanoparticles.

## Acknowledgements

We would like to thank T. Mates for making the SIMS measurements and M. Hashimoto for making the STEM measurements. This work is supported by the Center for Energy Efficient Materials (CEEM), an Energy Frontier Research Center (EFRC) funded at UCSB by the Office of Basic Energy Sciences of the US Department of Energy.

## References

[1] J.M. Zide, D.O. Klenov, S. Stemmer, A.C. Gossard, G. Zeng, J.E. Bowers, D. Vashaee, A. Shakouri, Appl. Phys. Lett. 87 (2005) 112102.
[2] J.M.O. Zide, D. Vashaee, Z.X. Bian, G. Zeng, J.E. Bowers, A. Shakouri, A.C. Gossard, Phys. Rev. B 74 (2006) 205335.
[3] W. Kim, J. Zide, A. Gossard, D. Klenov, S. Stemmer, A. Shakouri, A. Majumdar, Phys. Rev. Lett. 96 (2006) 045901.
[4] G. Zeng, J.H. Bahk, J.E. Bowers, H. Lu, A.C. Gossard, S.L. Singer, A. Majumdar, Z. Bian, M. Zebarjadi, A. Shakouri, Appl. Phys. Lett. 95 (2009) 083503.
[5] C.J. Palmstrøm, S. Mounier, T.G. Finstad, P.F. Miceli, Appl. Phys. Lett. 58 (1990) 382.
[6] W.R.L. Lambrecht, Phys. Rev. B 62 (2000) 13538.
[7] S.J. Allen Jr., F. DeRosa, C.J. Palmstrøm, A. Zrenner, Phys. Rev. B 43 (1991) 9599.
[8] K.T. Delaney, N.A. Spaldin, C.G. Van de Walle, Phys. Rev. B 77 (2008) 235117.
[9] B. Clerjaud, J. Phys. C: Solid State Phys 18 (1985) 3615.
[10] I. Poole, K.E. Singer, A.R. Peaker, A.C. Wright, J. Cryst. Growth 121 (1992) 121.
[11] S. Députier, R. Guérin, Y. Ballini, A. Guivarc'h, J. Alloys Compds. 202 (1993) 95.
[12] R.G. Wilson, F.A. Stevie, C.W. Magee, Secondary ion mass spectrometry: a practical handbook for depth profiling and bulk impurity analysis, Wiley, 1989.

[13] A. Shakouri, M. Zebarjadi, Nanoengineered materials for thermoelectric energy conversion, in: S. Volz (Ed.), Thermal Nanosystems and Nanomaterials, Springer-Verlag, Berlin Heidelberg2009, pp. 225–299.
[14] A.T. Ramu, L.E. Cassels, N.H. Hackman, H. Lu, J.M.O. Zide, J.E. Bowers, J. Appl. Phys. 107 (2010) 083707.
[15] D.C. Driscoll, M. Hanson, C. Kadow, A.C. Gossard, Appl. Phys. Lett. 78 (2001) 1703.
[16] I.V. Markov, Growth for beginners: fundamentals of nucleation, crystal growth, and epitaxy, 2nd, World Scientific Publishing Co., 2004.
[17] D.O. Klenov, D.C. Driscoll, A.C. Gossard, S. Stemmer, Appl. Phys. Lett. 86 (2005) 111912.
[18] B.D. Schultz, C.J. Palmstrøm, unpublished.